# Analysis and Model-based Control of Servomechanisms with Friction

Evangelos G. Papadopoulos and Georgios C. Chasparis

*Department of Mechanical Engineering*
*National Technical University of Athens, 15780 Athens, Greece*

## Abstract

*Friction is responsible for several servomechanism problems, and their elimination is always a challenge for control engineers. In this paper, feedback model-based compensation of friction is used for servomechanism set point and tracking tasks. Basic friction models are tested and their influence on system response is examined using describing function analysis. Analytical predictions are compared to simulation and experimental results. Various control laws using friction compensation were compared experimentally. Results showed that for both types of tasks, the best response is obtained by a model-based control law with friction compensation using the general kinetic friction model.*

## 1. Introduction

Friction is one of the greatest obstacles in high precision positioning systems. It can cause steady state and tracking errors, while it may result in limit cycles. Therefore, its influence on the response of systems, such as a servomechanism, must be considered seriously.

A number of methods of friction compensation have been proposed in the past including feedback and feedforward compensation, [1]. These methods rely upon the exact knowledge of the friction model and its parameters making friction identification necessary.

Off-line identification of friction is described in [2], [3] and [4]. In [2] a very simple technique is suggested in which static friction is measured by a number of breakaway experiments. This technique was applied to a complex mechanism, with the addition of measuring the static friction as a function of position, [3]. To find the friction-velocity relationship, several constant velocity motions were used in [3], [4].

Many friction models have been proposed that differ on the friction effects that are modeled in lubricated contact. These models can be divided into three categories. The first one includes the steady state friction models, where friction is a function of velocity, [1], [5], [6], and [7]. The second one includes time-dependent friction models, where friction effects, such as rising static friction, are included, [1]. Finally, the third one includes state friction models, which embody the natural mechanism of friction generation, [1], [5].

Kinetic friction models, such as the classical or the general kinetic friction models, are simpler than other models, [1], [5], [7]. Although these do not include dynamic friction effects, they tend to be sufficient for large displacement tasks, [7]. In addition, because they are simpler and not based on complex algorithms, they do not require large computing power, [7].

A problem with friction compensation is that always there may be a slight mismatch that may affect positioning and tracking accuracy or cause oscillations. Therefore, the effect of the mismatch to system response must be studied. Single-Input Describing Function Analysis (SIDF) is one of the basic tools for analyzing systems with nonlinearities such as friction, [1]. According to [1], two methods exist in which describing function analysis can be applied, i.e. the memoryless element construction and the integrated friction/plant construction. The conditions for limit cycle generation, according to the first method, in the case of PID control with Coulomb friction and with Coulomb plus static friction are examined in [8]. The validity of these results is also examined in [1], [8] and [10]. Moreover, the conditions needed to avoid limit cycles resulting from overcompensation when Coulomb friction is used as the basis for friction compensation are examined in [9].

In this paper, the classic Coulomb friction model and the general kinetic friction model are used for reducing steady state and tracking errors in a servomechanism control system. Steady state friction parameters are identified experimentally as a function of current position and velocity. Next, SIDF analysis is employed to predict limit cycle generation due to friction compensation, and design guidelines on the use of friction compensation are established. The validity of the quantitative predictions of this analysis is validated with simulation and experimental results.

Finally, friction compensation is employed in servo tasks such as step input and tracking commands. Various classical, model-based and friction compensating control laws are implemented and compared experimentally. Results show that for both types of commands, the best response is obtained by a model-based control law with friction compensation based on the general kinetic friction model.

## 2. Basic Friction Models

Steady state friction models, which are also called "static friction models" or "kinetic friction models", compute friction torque as a function of slowly varying velocity. The classical friction model is described by the following equation:

$$T_f = T_C \operatorname{sgn}(\dot{\theta}) + b\dot{\theta} \qquad (1)$$

where $T_C$ is the Coulomb friction level, $b$ is the viscous friction coefficient, and

$$\mathrm{sgn}(\dot{\theta})=\begin{cases}+1, & \dot{\theta}>0\\ 0, & \dot{\theta}=0\\ -1, & \dot{\theta}<0\end{cases} \quad (2)$$

If static friction is added to this model, the classical friction model is complete. According to this model, during stick, friction force can be modeled as a function of the external force, i.e.,

$$T_{stick}=\begin{cases}T_e, & |T_e|<T_s,\ \dot{\theta}=0,\ \ddot{\theta}=0\\ T_s\,\mathrm{sgn}(T_e), & |T_e|>T_s,\ \dot{\theta}=0,\ \ddot{\theta}\neq 0\end{cases} \quad (3)$$

where $T_e$ is the external torque, and $T_s$ is the breakaway torque, which is the limit between static friction and kinetic friction. The classical elements of friction can be combined in different ways, as shown in Fig. 1(a). All combinations are still considered classical models.

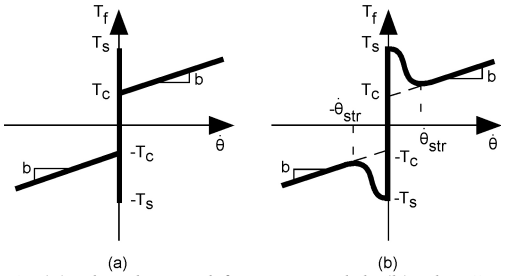


***Fig. 1****: (a) The classical friction model, (b) The General Kinetic Friction (GKF) model.*

However, the friction force which rises from the breakaway level to the Coulomb level is not discontinuous, but it is a function of velocity, [1]. This continuous dependence of friction on velocity is usually called the *Stribeck* curve or the *General Kinetic Friction* (*GKF*) model, see Fig. 1(b), and is described by,

$$T_f=\begin{cases}T_f(\dot{\theta}), & \dot{\theta}\neq 0\\ T_e, & \dot{\theta}=0,\ \ddot{\theta}=0,\ |T_e|<T_s\\ T_s\,\mathrm{sgn}(T_e), & \dot{\theta}=0,\ \ddot{\theta}\neq 0,\ |T_e|>T_s\end{cases} \quad (4)$$

A number of different parameterizations of this curve are quoted in [1], one of which is given below,

$$T_f(\dot{\theta})=\left[T_C+(T_s-T_C)\exp\left(-\left|\dot{\theta}/\dot{\theta}_{str}\right|^2\right)\right]\cdot\mathrm{sgn}(\dot{\theta})+b\dot{\theta} \quad (5)$$

In general, kinetic friction models cannot clearly distinguish the region of zero velocity, which is of vital importance during experiments. A solution to that problem was proposed by Karnopp, [6]. In particular, he developed a model, which specifies an interval in which the velocity can be considered as zero, thus avoiding the switching between sticking and sliding.

## 3. Friction Identification

To be able to test experimentally control laws in the presence of friction, an experimental servomechanism device was used. Motion is achieved by means of a roller-screw driver with a fixed centered carriage, see Fig. 2. A 48V, 70W DC motor with a torque constant of $K_T=0.105\ Nm/A$ is driven by a PWM current mode amplifier with gain $K_{amp}=0.4A/V$. The motor is equipped with a 500 count/rev encoder, resulting in a 42μm carriage positional accuracy. To avoid differentiation problems, a small DC motor, with a back-emf constant $K_{gen}=4.46\times10^{-3}V\,\mathrm{sec}/rad$, is used as a tachometer feeding back screw angular velocity, filtered by a 4 Hz low pass filter. The encoder and tachometer signals are read by a motion controller card (GALIL DMC-1700), interfaced to a 500 MHz Pentium III PC running the QNX real-time operating system.

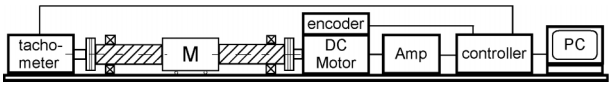


***Fig. 2****: Servomechanism configuration, including sensors, amplifier and controller.*

Two different experiments were designed in order to identify friction parameters as a function of carriage position; the first one was designed to yield the breakaway friction torque, while the second one to yield the steady state friction parameters. The experiments were conducted in an automated and unattended fashion during servomechanism idling time.

In the first experiment, the carriage was positioned at one of the sides of the roller-screw driver. Via a control program, the control voltage was increased gradually at a small step of 10 mV per 1 ms. When the encoder read a very small displacement (set at 10 encoder counts) the position and static control voltage were recorded. After the carriage came to rest for 20 s, a new experiment was initiated. When the carriage reached the other side of the roller-screw driver, the direction of the motion reversed. In this way, the static friction level for the other direction of motion was also measured.

In the second experiment, the control voltage for a constant carriage velocity motion was measured as a function of carriage position. The constant velocity was achieved with a simple PD controller. Several constant velocities were used and the mean values are shown in Fig. 3. The zero-velocity control voltages (currents) were obtained by the previous experiment.

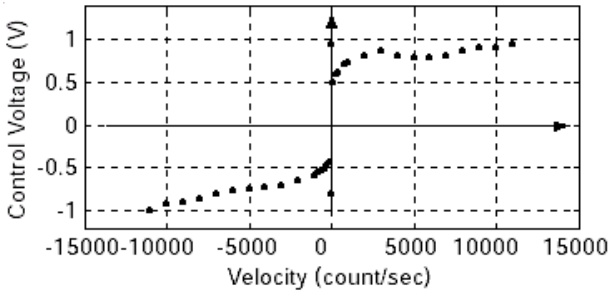


***Fig. 3****: Mean control voltage for several velocities.*

Due to the low sensor accuracy, very low constant velocities cannot be easily achieved and the friction rise curve in this region (boundary and partial lubrication regime, [1]) is not distinguishable. Nevertheless, the friction fall can be considered to be exponential.

Plots such as the one in Fig. 3 were obtained for a number of closely located carriage positions, by measuring control voltages (currents) when the carriage was passing through the position of interest. Curve

fitting the experimental points, with the kinetic friction models described in Section 2, can be done with the minimum error only for velocities lower than approximately 5000 count/sec because of a system nonlinearity at this velocity. These parameters are depicted as a function of carriage position accompanied with the standard deviation, see Fig. 4. As shown in this figure, friction parameters are slightly different between the positive and negative directions of motion.

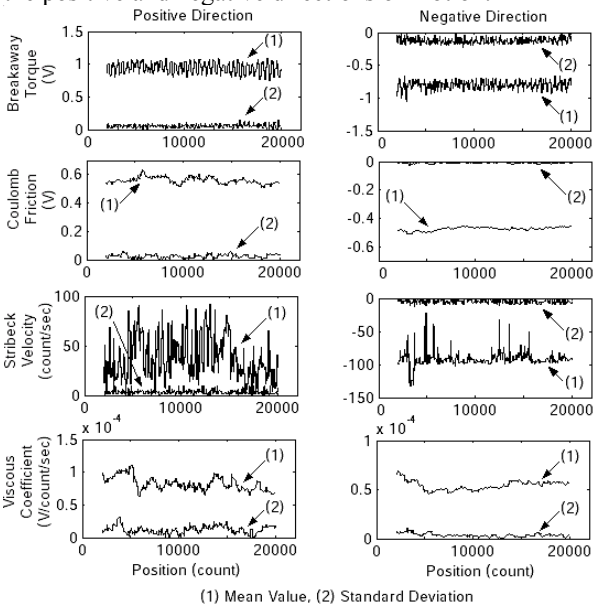


***Fig. 4**: Friction parameters and their standard deviation versus position.*

Finally, the effective inertia of the system was estimated from its transient response. To a good approximation, the open loop system is a first order system when its output is velocity. When the input signal is a step voltage, then the inertia can be measured from the time constant of the system and its viscous friction coefficient. Ten transient step response experiments were executed which yielded the following mean value of inertia,

$$\hat{J} = 2.14 \times 10^{-4}\, Kg\, m^2 \qquad (6)$$

## 4. Limit Cycle Analysis and Prediction

Before using friction compensation, one must analyze its effects in a closed-loop system and avoid situations in which this compensation may result in adverse response characteristics, such as limit cycles. To this end, SIDF analysis is employed.

Fig. 5 depicts the block diagram of a typical closed-loop servomechanism system in which friction compensation has been added. In this system, feedback consists of a state-feedback (PD) part and of an on-line model-based friction compensation term, $\hat{T}_f$.

It is assumed here that both the plant friction, $T_f$, and the friction compensation term, $T_f$, are described by the classic Coulomb friction model, given by Eq. (1).

To test for the existence of limit cycles, a SIDF approximation for the friction nonlinearity is used,

$$N(X) = 4 / \pi X \qquad (7)$$

where $N(X)$ is the describing function of $\mathrm{sgn}(\theta)$, and $X$ is the associated amplitude of oscillation, [11]. Using Eq. (7) and the block diagram in Fig. 5, the closed-loop characteristic equation is found to be

$$Js^2 + \left(\Delta b + \Delta T_C N(X) + K_d K_{amp} K_T\right)s + K_p K_{amp} K_T = 0 \quad (8)$$

with, $$\Delta T_C = T_C - \hat{T}_C, \quad \Delta b = b - \hat{b} \qquad (9)$$

where $\Delta T_C$ is the parametric error in the level of Coulomb friction, and $\Delta b$ is the parametric error in the viscous coefficient of friction.

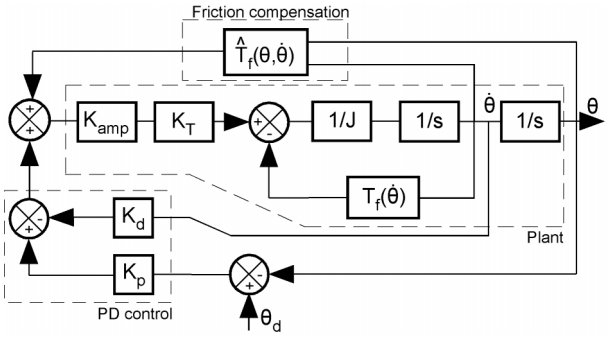


***Fig. 5**: Block diagram of the system with friction compensation and PD control.*

Applying the memoryless element construction, see [1], the non-linear part of the characteristic equation is separated from the linear part to yield,

$$\frac{-1}{N(X)} = \frac{\Delta T_C s}{Js^2 + \left(\Delta b + K_d K_{amp} K_T\right)s + K_p K_{amp} K_T} = G_{lin} \quad (10)$$

If Eq. (10) is satisfied for some oscillation frequency $\omega$ and some amplitude $X$, then a limit cycle will occur. Replacing $s$ with $j\omega$, and separating the real and imaginary parts yields,

$$\mathrm{Re}\{G_{lin}\} = \frac{\Delta T_C \omega^2 \left(\Delta b + K_d K_{amp} K_T\right)}{\left(\Delta b + K_d K_{amp} K_T\right)^2 + \left(-J\omega^2 + K_p K_{amp} K_T\right)^2} \quad (11)$$

$$\mathrm{Im}\{G_{lin}\} = \frac{\Delta T_C \omega \left(-J\omega^2 + K_p K_{amp} K_T\right)}{\left(\Delta b + K_d K_{amp} K_T\right)^2 + \left(-J\omega^2 + K_p K_{amp} K_T\right)^2} \quad (12)$$

Since the left hand-side term in Eq. (10) is always a negative real number, and since

$$K_p, K_d, K_T, K_{amp}, J > 0 \qquad (13)$$

a limit cycle will be generated if and only if

$$\mathrm{Re}\{G_{lin}\} < 0 \Leftrightarrow \Delta T_C \left(\Delta b + K_d K_{amp} K_T\right) < 0 \quad (14)$$

According to the Routh-Hurwitz stability criterion, the same closed loop system but without friction, is unstable if and only if

$$\Delta b + K_d K_{amp} K_T < 0 \qquad (15)$$

Thus, we may conclude that when there is no Coulomb friction compensation or when $\Delta T_C > 0$, a limit cycle will be generated if and only if the system without the non-linear part of friction is unstable. This result applies not only in the presence of plant friction, as suggested in [8], but also in the presence of friction compensation terms included in $T_f$. Based on Eq. (14), Table 1 is generated summarizing the conditions under which a limit cycle will be generated.

According to Eqs. (10), (11), and (12), the amplitude $X_{LC}$ and frequency $\omega_{LC}$ of the generated limit cycle will be,

$$X_{LC} = -\frac{4}{\pi}\cdot\frac{\Delta T_C}{\left(\Delta b + K_d K_{amp} K_T\right)},\ \omega_{LC} = \sqrt{\frac{K_p K_{amp} K_T}{J}} \quad (16)$$

***Table 1:*** *Limit cycle generation map.*

| | $\Delta b > 0$ | $\Delta b < 0$ |
|---|---|---|
| $\Delta T_C > 0$ | Never | If $K_d < -\Delta b / K_{amp} K_T$ |
| $\Delta T_C < 0$ | Always | If $K_d > -\Delta b / K_{amp} K_T$ |

However, according to the conditions for the validity of the describing function predictions, see [11], Eqs. (16) yield satisfactory results if and only if the linear part of the system attenuates adequately the higher harmonics.

This suggests that before drawing conclusions regarding the behavior of the system using a SIDF, the range of validity of the criterion must be established. To this end, note that since the non-linearity in Eq. (7) is an odd function, the ratio of two neighboring harmonics will be three. This observation allows us to define a criterion for applying the SIDF method. We define a measure $\Delta G$ which is equal to the difference in the logarithmic magnitude of the linear part, given by Eq. (11), evaluated at the basic harmonic of a limit cycle, $\omega_{LC}$, and the same magnitude evaluated at the next higher harmonic, $3\omega_{LC}$,

$$\Delta G = 20\left\|\log|G_L(j\omega_{LC})| - \log|G_L(j(3\omega_{LC}))|\right\| \quad (17)$$

To examine the correlation of this measure to SIDF predictions, extensive simulations and experiments were carried out. Simulations took place in Matlab / Simulink where the mean experimental values for friction parameters were used. The input command was a step of 4000 counts. In simulations, the various values of $K_p$, $K_d$, $\Delta b$, $\Delta T_C$ used as well as the resulting values for the value of the measure $\Delta G$ were recorded. Estimates for the real values of $b$ and $T_C$ used were obtained by multiplying the mean experimental estimates $\hat{b}$ and $\hat{T}_C$, with a number greater than one. However, this may result in discrepancies between the real $\Delta b$ and $\Delta T_C$, and the ones used in simulation.

Table 2 displays the theoretical values for limit cycle amplitudes and frequencies for various combinations of $K_p, K_d, \Delta b, \Delta T_C$.

The simulation runs were also tried experimentally. A comparison between simulation and experiments is given in Table 3. Based on the results in Table 3, the error of evaluating the theoretical limit cycle amplitude and frequency for both simulation and experiment is plotted as a function of $\Delta G$ in Fig. 6. Table 3 and Fig. 6 show that the describing function analysis predicts well limit cycle amplitude and frequency as long as the logarithmic difference $\Delta G$ is greater than 20 dB.

Experimental measurements support this conclusion for amplitudes lower than almost 5000 count/sec or 62.8 rad/sec, where friction has been modeled with good approximation.

***Table 2:*** *Limit cycle amplitude and frequency values according to the describing function analysis.*

| Case No | $K_p$ $\frac{V}{rad}$ $\times 10^{-1}$ | $K_d$ $\frac{Vs}{rad}$ $\times 10^{-2}$ | $\Delta T_C$ $Nm$ $\times 10^{-2}$ | $\Delta b$ $\frac{Nms}{rad}$ $\times 10^{-4}$ | $\Delta G$ $dB$ | $X_{LC}$ $\frac{rad}{\sec}$ | $\omega_{LC}$ $\frac{rad}{\sec}$ |
|---|---|---|---|---|---|---|---|
| 1 | 3.98 | 15.9 | -4.14 | -4.36 | 2.18 | 8.43 | 8.84 |
| 2 | 3.98 | 11.9 | -4.14 | -4.36 | 3.45 | 11.5 | 8.84 |
| 3 | 3.98 | 7.96 | -4.14 | -4.36 | 6.03 | 18.1 | 8.84 |
| 4 | 3.98 | 6.37 | -4.14 | -4.36 | 7.83 | 23.5 | 8.84 |
| 5 | 3.98 | 4.78 | -4.14 | -4.36 | 10.5 | 33.6 | 8.84 |
| 6 | 3.98 | 2.39 | -4.14 | -1.01 | 15.1 | 58.5 | 8.84 |
| 7 | 3.98 | 1.59 | -4.14 | -1.01 | 19.0 | 92.9 | 8.84 |

***Table 3:*** *Simulation and Experimental values of limit cycle amplitude and frequency*

| Case No | Simulation | | | | Experiment | | | |
|---|---|---|---|---|---|---|---|---|
| | $X_{LC}$ | $e_X$ (%) | $\omega_{LC}$ | $e_\omega$ (%) | $X_{LC}$ | $e_X$ (%) | $\omega_{LC}$ | $e_\omega$ (%) |
| 1 | 11.1 | 31.6 | 1.10 | 87.6 | 11.3 | 34.1 | 6.12 | 30.8 |
| 2 | 14.0 | 21.7 | 1.76 | 80.1 | 14.6 | 27.0 | 5.84 | 33.9 |
| 3 | 18.8 | 3.87 | 5.67 | 35.9 | 21.6 | 19.3 | 6.18 | 30.1 |
| 4 | 24.5 | 4.26 | 7.18 | 18.8 | 22.9 | 2.55 | 7.11 | 19.6 |
| 5 | 31.9 | 5.06 | 8.01 | 9.39 | 27.9 | 17.0 | 8.50 | 3.85 |
| 6 | 56.1 | 4.10 | 8.59 | 2.82 | 62.9 | 7.52 | 10.4 | 17.6 |
| 7 | 90.6 | 2.48 | 8.74 | 1.13 | 127 | 36.7 | 11.2 | 26.7 |

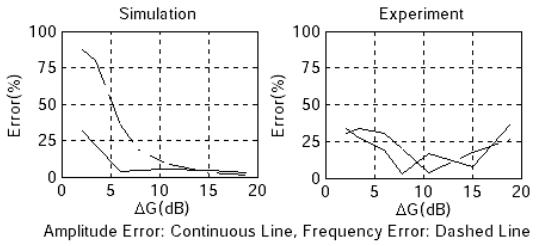


***Fig. 6****: Simulation and Experimental SIDF prediction errors for limit cycle amplitude and frequency.*

It can be shown and was demonstrated experimentally that the conditions for limit cycle generation do not depend on the inclusion of static friction in the friction model used. Static friction, as described by Eq. (3), is important during the beginning of system motion, [12].

## 5. Model-Based Control with Friction Models

Having the friction models and their experimentally obtained parameters, various control laws were set-up and evaluated for steady state and tracking response tasks. For these laws, friction parameters in the control laws were chosen such that limit cycles would never occur. The first friction model employed is the Coulomb plus viscous friction (CV) model, described by Eqs. (1) and (2), slightly modified to deal with the difficulty of identifying zero velocities,

$$\hat{T}_{f,cv} = \hat{T}_C\ \ f(\dot{\theta}) + \hat{b}\,\dot{\theta} \quad (18)$$

where:
$$f(\dot\theta)=\begin{cases}+1, & \dot\theta>\Delta\dot\theta\\ 0, & |\dot\theta|\le\Delta\dot\theta\\ -1, & \dot\theta<-\Delta\dot\theta\end{cases} \quad (19)$$

and $\Delta\theta = 40\ counts/\sec = 0.503\ rad/\sec$, i.e. a very small velocity.

The second friction model is the GKF model,

$$\hat T_{f,gk}=\left[\hat T_C+\left(\hat T_s-\hat T_C\right)\exp\left(-\left|\dot\theta/\hat{\dot\theta}_{str}\right|^2\right)\right]f(\dot\theta)+\hat b\dot\theta \quad (20)$$

where $f(\theta)$ is defined by Eq. (19). In both models, all parameters are functions of carriage position.

### 5.1 Steady-state position error

Three control schemes were used to study the reduction of steady state position error that friction compensation causes. These include,

- *Proportional-Derivative/state feedback (PD)*,
$$T_{pd}=K_p(\theta_d-\theta)-K_d\dot\theta=K_pe-K_d\dot\theta \quad (21)$$
- *PD with Coulomb and viscous friction model* given by Eq. (18), (PDCV),
$$T_{pdcv}=T_{pd}+\hat T_{f,cv} \quad (22)$$
- *PD and General Kinetic Friction model* given by Eq. (20), (PDGK),
$$T_{pdgk}=T_{pd}+\hat T_{f,gk} \quad (23)$$

All control algorithms were written in C and executed at a 4 ms loop-time under QNX. To be able to use model-based friction compensation the controller card PID controller was by-passed and the card was only used for reading current position and velocity from the encoder and tachometer, respectively, and for sending the appropriate control voltage to the amplifier.

The PD gains for the PD law have been chosen so that the closed-loop system is critically damped with a closed-loop frequency equal to 17.67 rad/s,

$$\omega_{cl}=\sqrt{\frac{K_TK_{amp}K_p}{\hat J}}=17.67\frac{rad}{\sec},\zeta_{cl}=\frac{\hat b+K_TK_{amp}K_d}{2\hat J\omega_{cl}}=1 \quad (24)$$

This yields the following gains,

$$K_{p,pd}=1.592V/rad,\quad K_{d,pd}=0.175V\sec/rad \quad (25)$$

The PD gains for the other two algorithms were selected so that, if friction is perfectly compensated, the closed-loop system is critically damped, and the control voltage level is about the same for all three schemes. These constraints yielded the following gains,

$$K_p=1.592V/rad,\quad K_d=0.180V\sec/rad \quad (26)$$

For all three schemes, the desired displacement was $\theta_d = 6000\ counts$ and was achieved by a triangle velocity profile.

Typical error responses of these control schemes accompanied with the respective control voltages are shown in Fig. 7. Repeating the same experiments for ten consecutive times, the mean steady-state errors for each algorithm were computed and are shown in Table 4.

Comparing these results, it is obvious that the PDGK control scheme is superior to the PDCV and the classic PD control laws. In particular, the PDGK reduces the steady state error almost 10 times compared to a classical PD law. Also, it was observed that the introduction of the breakaway torque to a friction model reduces the steady state error.

***Table 4:*** *Mean value and standard deviation of steady-state position error for the control schemes in Sect. 5.1.*

| | PD | PDCV | PDGK |
|---|---|---|---|
| Mean Value | 25.2 | 13.7 | 2.70 |
| Standard Deviation | 5.07 | 5.83 | 2.54 |

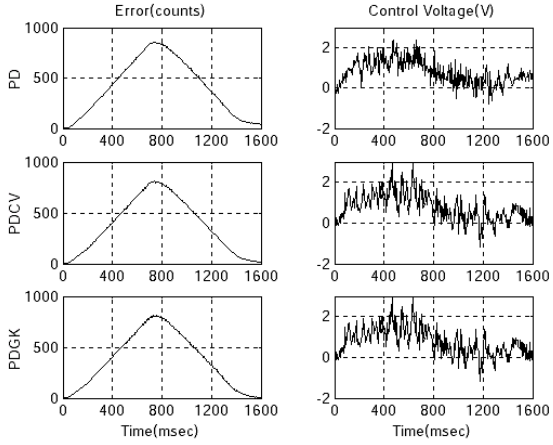


***Fig. 7****: Typical error responses with the respective control voltage.*

### 5.2 Tracking error

In order to examine the improvement of tracking error response with friction compensation, five control schemes were employed. The command was based on a triangle velocity profile. Except the PD and PID, the other laws include additional model-based estimates of the carriage inertia to improve the tracking response without the use of large control gains. The PD law is the same as in Section 5.1. The remaining the laws include,

- *Proportional-Derivative-Integral*, (PID),
$$T_{pid}=K_pe+K_d\dot e+K_i\int_0^t e(t)dt \quad (27)$$
- *Model-Based Control,* (MB),
$$T_{mb}=\hat J\ddot\theta_d+K_d\left(\dot\theta_d-\dot\theta\right)+K_p(\theta_d-\theta)=\\ =\hat J\ddot\theta_d+K_d\dot e+K_pe \quad (28)$$
- *MB and Coulomb and Viscous Friction model,* (MBCV),
$$T_{mbcv}=T_{mb}+\hat T_{f,cv} \quad (29)$$
- *MB and General Kinetic Friction model*, (MBGK),
$$T_{mbgk}=T_{mb}+\hat T_{f,gk} \quad (30)$$

The block diagram of the closed-loop system with the various model-based schemes is shown in Fig. 8. The PD, MB, MBCV and MBGK laws are executed under QNX, as described in Section 5.1. The gains $K_p, K_d$ have been chosen for critical closed-loop damping, and for a frequency equal to 17.67 rad/s. The PID control was executed by a loop implemented on the motion

controller card. The PD and PID gains were chosen so that the bandwidth and the control voltage level is at the same level with that of the other controllers.

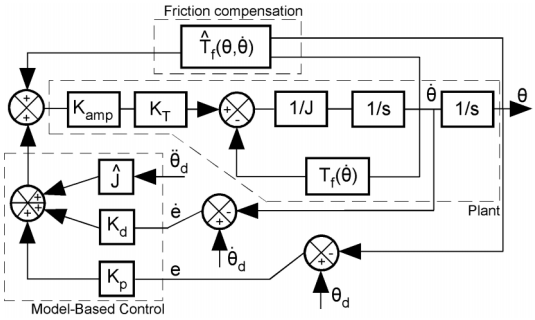


***Fig. 8**: Model-Based Control with compensation of friction.*

Typical tracking errors and control voltages are given in Fig. 9. As shown in this figure, the PD law results in excessive tracking errors, as expected. The PID law tracking error is of the order of 20 counts and shows poor tracking during the acceleration and deceleration phases. However, it drives the steady state error to ±1 counts, due to the integral action.

The MBGK reduces the tracking error below 10 counts throughout the motion, which is 10 times better than the PD performance. This law is better in comparison to MBCV at the beginning and at the end of the trajectory because it includes the breakaway torque. Although these laws include no integral action, they exhibit very good performance even at the steady state. Adding integral action to these algorithms can eliminate the steady-state error to the level of the PID law.

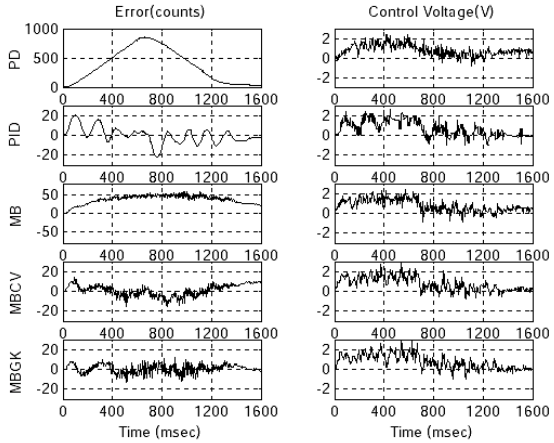


***Fig. 9**: Typical error responses and the corresponding control voltage.*

These results show that model-based control laws with friction compensation are beneficial for both steady state and tracking response. Undesirable limit cycles were eliminated by the proper choice of friction parameters. The fact that they do not require additional feedback makes them attractive for improving system response with software components only.

## 6. Conclusions

In this paper, the classic Coulomb friction and the general kinetic friction models as a function of position were used for reducing steady state and tracking errors in a servomechanism control system. Steady state friction parameters were identified experimentally as a function of current position and velocity. Next, SIDF analysis was employed to predict limit cycle generation due to friction compensation, and guidelines on the use of friction compensation were established. The validity of the quantitative predictions of this analysis was demonstrated with simulation and experimental results. Friction compensation was employed in servo tasks such as steady-state response and tracking. Various classical, model-based and friction compensating control laws were implemented and compared experimentally. Results showed that for both types of commands, the best response was obtained by a model-based control law with friction compensation based on the general kinetic friction model.

## References


[1] Armstrong-Helouvry, B., P. Dupont and C. Canudas de Wit, "A Survey of Models, Analysis Tools and Compensation Methods for the Control of Machines with Friction," *Automatica*, Vol. 30(7), 1994, pp. 1083-1138.

[2] Armstrong, B., *Control of Machines with Friction*, Kluwer Academic Publishers, Boston, USA, 1991.

[3] Popovic, M. R. and Goldenberg, A. A. "Friction diagnostics and modeling using DFT analysis," *Proc. 1997 IEEE Conference on Robotics and Automation*, Albuquerque, New Mexico, April 1999.

[4] Ro, I. P., Wonbo Shim and Sanghwa Jeong, "Robust friction compensation for submicrometer positioning and tracking for a ball-screw-driven slide system", *Positioning Engineering*, 24, 2000, pp. 160-173.

[5] Olsson, H., et al., "Friction Models and Friction Compensation", *J. of Europ. Control*, Vol. 4(3), 1998.

[6] Karnopp, D., "Computer simulation of stick-slip friction in mechanical dynamic systems", *ASME J. of Dynamic Systems, Measurement and Control,* 1985, 107(1), 100-103.

[7] Altpeter, F., F. Ghorbel and R. Longchamp, "Relationship Between Two Friction Models: A Singular Perturbation Approach", *Proc. 37th IEEE Conference on Decision & Control*, Tampa, Florida USA, December 1998.

[8] Armstrong-Helouvry, B. and Amin, B., "PID Control in the Presence of Static Friction: Exact and Describing Function Analysis," *Proc. American Control Conference*, Baltimore, Maryland, June 1994.

[9] Canudas de Wit, C., P. Noël, A. Aubin and B. Brogliato, "Adaptive Friction Compensation in Robot Manipulators: Low Velocities," *Int. Journal of Robotics Research*, Vol. 10, No. 3, June 1991.

[10] Armstrong, B. and Amin, B., "PID Control in the Presence of Static Friction: A Comparison of Algebraic and Describing Function Analysis", *Automatica*, Vol. 32, No 5, 1996, pp. 679-692.

[11] Ogata, K., *Motion Control Engineering*, Prentice Hall, Englewood Cliffs, NJ, 1970.

[12] Chasparis, G., "Design of Servomechanism Control System with Friction Compensation," (in Greek), *Master's Thesis,* Dept. of Mechanical Engineering, NTUA, Athens, Greece, 2001.